JCIS Open 20 (2025) 100154

Contents lists available at ScienceDirect

JCIS Open

journal homepage: www.journals.elsevier.com/jcis-open

Influence of wettability on diffusion limited nanoparticle adsorption at gas-liquid interfaces

Hangyu Chen [a,b,*], Xiaodong Jia [a], Michael Fairweather [a], Timothy N. Hunter [a,**]

[a] School of Chemical and Process Engineering, University of Leeds, Leeds, LS2 9JT, United Kingdom
[b] Department of Engineering Mechanics, Tsinghua University, Beijing, 100084, China

ARTICLE INFO

Keywords:
Colloidal adsorption
Hydrophobicity
Surface tension
Adsorption dynamics

ABSTRACT

This study investigates the influence of hydrophobicity on particle adsorption by examining the behavior of hydrophobized silica particles at air-water interfaces. Langmuir-Blodgett (LB) trough studies of butanol ('SiO-butane') and hexanol ('SiO-hexane') esterified particles provided contrasting behavior. The SiO-butane particles formed weaker particle layers that underwent partial collapse with compression, leading to formations significantly below hexagonal close-packed estimates. In contrast, the SiO-hexane particles exhibited improved monolayer behavior and longer-range stability. Droplet surface tensions demonstrated that the hydrophobic particles significantly altered the dynamic tension during adsorption, when methyl isobutyl carbinol (MIBC) was added as a co-surfactant. Short-term modeling elucidated the role of diffusion and energy barriers on adsorption dynamics, with SiO-hexane having reduced diffusion coefficients with respect to SiO-butane and unmodified particles. Despite this reduced diffusion, long-term modeling allowed calculation of adsorption coefficients (k_a), which for SiO-hexane particles were ~200 × greater than for unmodified particles at low 0.1 wt% particle concentrations and over 1000 × greater at 2 wt%. Overall, the results provide quantitative insights into the profound influence of hydrophobicity on particle adsorption, particularly in crowded surface environments. Importantly, a diffusion-only mechanism is inadequate to explain adsorption dynamics for these larger colloids and the gravity-driven contribution must be considered in early-stage kinetics.

1. Introduction

Colloidal particle adsorption at liquid interfaces holds significant importance in diverse industries, including printing [1,2], cosmetics [3,4] and drug delivery [5]. Surface tension is an important property of the gas-liquid interface and it arises from the energetic disparities between molecules residing at fluid interfaces and those within the bulk, operating intricately at the molecular scale [6]. The excess energy present at the surface, known as surface free energy, can be quantitatively expressed as energy per unit area [7]. Colloidal particles, measuring typically from several nanometers to hundreds of nanometers in diameter, possess the capability to adsorb at liquid interfaces, thus modifying the 'apparent' surface tension [8,9]. When colloidal particles adsorb at fluid-fluid interfaces, they exhibit distinct physical and chemical behaviors that can impact the mechanical properties of the interface [10–12].

The nanoparticle adsorption process is normally deemed irreversible, and so unlike surfactants, is shaped by various factors including particle radius and wettability [13–15]. Thermodynamically, the adsorption of moderately hydrophobic nanoparticles at liquid interfaces is greatly favored, unless they are highly charge stabilized. However, kinetic constraints can limit this process, posing a significant energy barrier to adsorption [16]. As adsorption at the interface reaches saturation, the networking of adsorbed particles becomes critical [17,18]. Both initial adsorption and the surface saturation stage are influenced by the electrostatic interaction [19–21]. To investigate the collapse behavior of nanoparticle layers with varying wettability, Langmuir-Blodgett troughs [22,23] are a valuable tool, enabling the study of adsorbed monolayers and multilayers of surface-active species. For example, previous studies on fumed silica particle layers have explored the influence of hydrophobicity on surface pressure measured with a Langmuir trough [11,24]. This technique allows for a qualitative analysis of the particle layers throughout the compression-expansion process.

* Corresponding author. School of Chemical and Process Engineering, University of Leeds, Leeds, LS2 9JT, United Kingdom
** Corresponding author.
E-mail addresses: chenhangyu1henry@163.com (H. Chen), t.n.hunter@leeds.ac.uk (T.N. Hunter).

https://doi.org/10.1016/j.jciso.2025.100154
Received 16 July 2025; Received in revised form 2 September 2025; Accepted 5 September 2025
Available online 6 September 2025

The shape of nanoparticles is known to considerably influence their diffusion and arrangement at gas-liquid interfaces, as demonstrated by the experimental surface tension results of Kumar et al. [25]. However, to simplify investigations, a focus on spherical particles allows for a more quantitative analysis of surface monolayers, with reference to theoretical hexagonal close-packed structures. To assess the adsorption rate and kinetics of colloidal particles, dynamic surface tension measurements can be used [11,25–27]. Surface or interfacial tension has proven to be an effective measurable indicator to track adsorption dynamics of nanoparticles at gas-liquid or liquid-liquid interfaces, as long as the apparent surface tension varies measurably with time [28]. Critical to the interpretation of these measurements is a suitable model that bridges the gap between dynamic surface tension and transient nanoparticle interfacial coverage [26]. Among the various methods for measuring surface tension, the pendant drop tensiometer stands out for its suitability in long-duration measurements [17]. This method, regarded as one of the most robust and versatile for tracking surface tension dynamically, involves suspending a fluid droplet from a needle [6]. By leveraging appropriate scaling, the axisymmetric Young-Laplace equation and drop character parameters, a relationship between drop shape and interfacial tension can be established [29]. For particle-laden droplets, variations in droplet volume can significantly influence the formation of particle layers during compression or extension. The particle layer structures may also change, affecting the accuracy of the adsorption measurement [27].

Importantly, Bizmark et al. [26] employed dynamic surface tension measurements to monitor the adsorption of ethyl cellulose nanoparticles at the gas-liquid interface. They combined a modified short-time adsorption model and early-time dynamic surface tension data with a separate long-time model to interpret data at equilibrium, enabling the calculation of the adsorption energy barrier and rate of nanoparticle adsorption. Notably, the surface tension exhibits a non-linear relationship with time, varying as $t^{0.5}$ and $t^{-0.5}$, reflecting distinct adsorption behaviors in the early and late stages. Similarly, Dugyala et al. [30] conducted research on the adsorption kinetics of nano-silica particles, utilizing dynamic surface tension measurements and a modified short-time model to estimate the energy barrier. The stability of the adsorption interface has also been investigated by Parajuli et al. [31], where they suggested the increased interfacial viscosity and elastic modulus typically contribute to greater interfacial stability. In most previous studies, the nanoparticles investigated are typically small enough for diffusion to dominate. Larger particles ($>$ 500 nm) that may have competing buoyancy effects have rarely been investigated.

Analyzing the intricate adsorption behavior of nanoscale particles remains a challenging task. Although simulations offer a promising path to exploring this phenomenon [32,33], empirically based theories still take precedence, where the collective influence of particle-interface dynamics can be related to changes in apparent surface tension. Central to this exploration is the three-contact line problem, which is crucial to understanding colloidal adsorption [34,35]. Therefore, in this study, the effect of particle wettability on the surface monolayer structure and rate of colloidal adsorption at an air-water interface was investigated. Relatively large silica nanoparticles (800 nm) were esterified to varying degrees to render different contact angles. Their compressional film formation was studied with a Langmuir-Blodgett trough, along with the competing influence of methyl isobutyl carbinol (MIBC) surfactant. The pendant drop tensiometry method was then used to measure adsorption, applying the short-time and long-time approximation models of Bizmark et al. [26]. Critically, this allows quantitative evaluation of the influence of wettability and particle concentration on the effective diffusion coefficient (D_{eff}) and adsorption rate (k_a).

2. Experimental section and methods

2.1. Materials

For convenience and ready availability, Angstrom Sphere® silica powder was used, with a nominal mean size of 800 nm (Fibre Optic Centre Inc., USA) consistent with previous research by the current authors [36,37]. To modulate the wettability of the silica particle surface, an esterification reaction was employed [38], which is known to produce an organic monolayer without secondary or polymerization reactions [39,40], thereby negating any significant changes in particle size. Two different long-chain alcohols, namely 1-butanol and 1-hexanol, were employed to hydrophobize silica particles to varying degrees. For ease of reference, the particles resulting from esterification with butanol and hexanol are designated as 'SiO-butane' and 'SiO-hexane', respectively. Direct measurement of the static contact angle of silica nanoparticles is impractical. Therefore, silica wafers were utilized to detect changes in contact angle resulting from esterification. Similar treatments were applied to polished silica wafers made of the same material as the silica particles. The contact angles of treated silica wafers were measured with a tensiometer (Theta tensiometer, Biolin Scientific, Finland). The measured contact angles for the unmodified SiO_2, SiO-butane, and SiO-hexane were 25.3°, 46.6° and 68.5° respectively. The values for SiO-butane and SiO-hexane wafer are similar to those previously reported for butanol and octanol esterified silica wafers [38]. Additionally, it is assumed they correlate closely to the contact angles of silica nanoparticles treated using the same method, due to the consistent density of formed monolayers from esterification.

2.2. Adsorption layer measurements and dynamic surface tension

A 150 mL KSV NIMA Langmuir trough (Biolin Scientific, Germany) was utilized to monitor alterations in surface pressure resulting from the reorganization of adsorbed nanoparticles. Prior to each measurement session, the trough underwent rigorous testing using deionized water sourced from a Milli-Q® system (Millipore Ltd., 18.2MΩ cm) as a standard, ensuring oscillations did not exceed 2 mN/m. Subsequently, the trough was filled with various concentrations of water and 4-methyl-2-pentanol (MIBC) subphases, a common surfactant in industrial applications, from 0.01 M to 0.05 M. A schematic representation of the Langmuir trough and the process of particle spreading are illustrated in the Electronic Supplementary Materials (ESM), Fig. S1.

After calibration, the Langmuir trough was filled with an aqueous phase volume of 70 mL, with a height of 5 mm. To deposit particle monolayers, a dispersion was first prepared by mixing dried particle powder in acetone at a concentration of 10 wt%. This mixture was initially processed using an ultrasonic probe (Sonic Dismembrator, Fisher Scientific) at 80 % amplitude for 3 min without heating. This was followed by a secondary treatment in an ultrasonic bath (XUBA3, Grant) for 5 min. The ultrasonic treatment followed a similar approach to that in the authors' previous work and proved sufficient for the breakup of aggregates, achieving a stable dispersion of spherical particles, without mechanically damaging the particles themselves [36]. The nanoparticle dispersion was then carefully deposited onto the water surface between the barriers of the trough using a microsyringe (Hamilton, 100 μL). Droplets were formed gently at the end of the needle and touched onto the surface to facilitate deposition (see ESM Fig. S1(b)).

To explore the disparity between theoretical hexagonal close-packed (HCP) structures and experimental results, a TM3030 Plus SEM (Hitachi High-Tech, USA) was employed to examine monolayers obtained from the Langmuir trough under varying surface pressures. Particle monolayers were extracted from the Langmuir trough interface at different surface pressures using the same suspension sample for comparison. The monolayer was obtained by using thin glass wafers pulled up through the surface. Subsequently, the samples were subjected to a 10 min drying period in an oven before being transferred to the SEM for

analysis.

The surface tension was measured using a Tensiometer CAM 200 (KSV Instruments Ltd., Finland). Surface tension versus time data were obtained by analyzing the curve of the droplet profile along with the recorded time. To reduce the influence of solvent evaporation, a closed cuvette was filled with 10 mL of solvent at the bottom and 3 mL of solvent in a large syringe, similar to the work of Saad et al. [41]. A droplet was prepared and suspended on the needle of the large syringe, before a 20 min waiting period was used to ensure saturation of the environment and stability of the droplet on the needle. Subsequently, the pendant droplet was injected with a minimum volume, typically around 8.5–9 μL. However, for suspensions with relatively low surface tension (high MIBC concentrations), the volume of the droplet could be smaller due to limitations in needle capacity.

Particles with varying hydrophobicity (Unmodified SiO_2, SiO-butane, and SiO-hexane) were used along with 0.03 M MIBC to ensure good surface tension response required to monitor adsorption dynamics. The surface tension of the 0.03M MIBC solution by itself was measured as 48.5 mN/m, showing good agreement with the work of other researchers [42].

Fig. 1 depicts the surface tension of a pure water droplet against the air in a close cuvette (not completely sealed) with a total volume of 10 mL, wherein 1 mL of water is injected using a larger syringe to facilitate an evaporation environment. At the commencement of the experiment, a test droplet of water or MIBC solution (marked as Drop 2) was prepared and suspended on the large needle. A few minutes were allowed for the establishment of a saturated atmosphere. The experiment was initiated once the test droplet reached a stable state with no noticeable change in volume. Subsequently, the measuring nanoparticle suspension drop (marked as Drop 1) was injected, marking the start of formal measurements.

2.3. Dynamic modeling of adsorption from surface tension data

The adsorption rate of colloidal particles can be analyzed by monitoring the surface tension change of the droplet. Since the actual position of nanoparticles with respect to the interface is difficult to measure, the contact angle of the silica nanoparticles used in the study was assumed to be that of the contact angle of silica wafers chemically esterified using the same method [38] (see ESM, Fig. S2 with detailed data in Table S1). The relationship between surface tension and the adsorption of particles at the interface is assumed to follow asymptotic behavior [43]. Thus, the asymptotic results are employed to interpret dynamic surface tension data from the early (short-time, $t\to0$) and late (long-time, $t\to\infty$) stages of nanoparticle adsorption as follows:

$$t\to 0 : \gamma = \gamma_0 - 2RTC_0\sqrt{\frac{Dt}{\pi}}, \tag{1}$$

$$t\to \infty : \gamma = \gamma_\infty + \frac{RT\Gamma_\infty^{-2}}{C_0}\sqrt{\frac{\pi}{4Dt}}, \tag{2}$$

where R is the gas constant (J/(mol·K)), T is the temperature (K), C_0 is the molar bulk concentration (M), Γ_∞ is the molar surface concentration at steady state (mol/m^2), and D is the nanoparticle diffusion coefficient (m^2/s).

Bizmark et al. [26] studied the kinetics of adsorption of small ethyl cellulose nanoparticles at the water-air interface. In particular, for $t\to 0$, usually called the 'early stage' of adsorption, the initial decay of surface tension is given by a modified short-time approximation as Eq. (3) [44],

$$\gamma = \gamma_0 - 2N_A C_0 \Delta E\sqrt{\frac{Dt}{\pi}}. \tag{3}$$

In this equation, γ is the interfacial tension (N/m) at any given time t (s), γ_0 is the pure solution interfacial tension (N/m), N_A is Avogadro's number, C_0 is the initial bulk concentration of particles (M) and ΔE is the detachment energy (J) of the particle [45]. The above equation assumes that the adsorption of particles at the interface is instantaneous. Bizmark et al. [26] also used Eq. (3) to fit the initial γ versus $\sqrt{t}$ data with ΔE as the fitting parameter for several initial concentrations of particles, C_0. In this study, the authors used the model of Bizmark et al., [26] to analyze the first stage of adsorption, which is mainly assumed to be dominated by particle diffusion.

Initially, adsorption is limited by the diffusion process as the interface is free of particles. Once nanoparticles adsorb to the interface it is very unlikely that they detach from the interface due to high detachment energy. Therefore, a modified diffusion-controlled theory is used to model the early time adsorption process. To include the energy barrier effects on the adsorption process, the particle diffusivity, D, is replaced with the effective diffusion coefficient, D_{eff}, in Eq. (3). Therefore, the effective diffusivity of the particles can be calculated by modelling the early time dynamic surface tension data using the adsorption kinetics model in Eq. (4) [44],

$$\gamma = \gamma_0 - 2N_A C_0 \Delta E\sqrt{\frac{D_{eff}t}{\pi}}. \tag{4}$$

Here, D_{eff} is the effective diffusion constant, and the equation can be expressed as a linear, according to Eq. (5):

$$\gamma = P_1 - P_2\sqrt{t}, \tag{5}$$

where P_1 is the pure solution interfacial tension (γ_0) and P_2 is

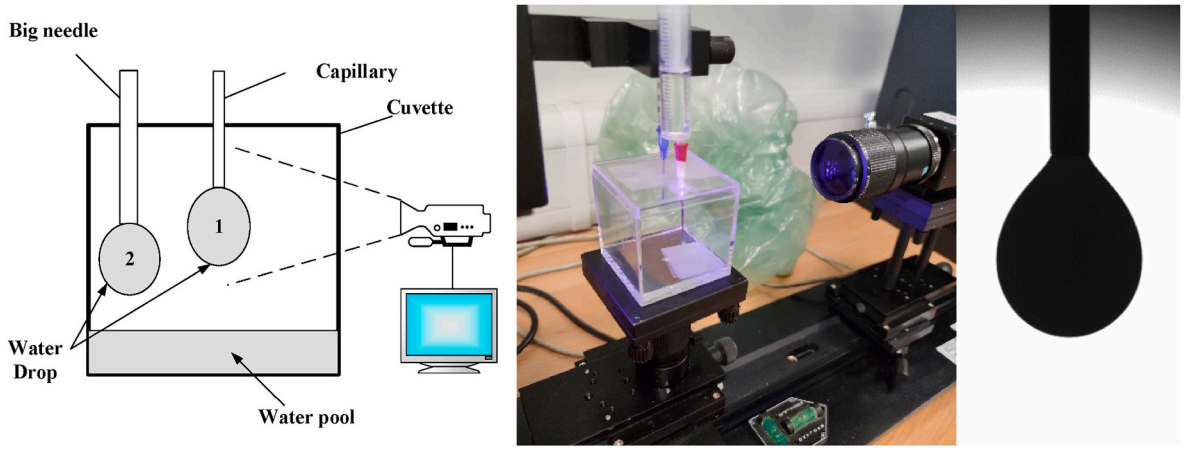

Fig. 1. Schematic of the pendant drop surface tension measurement setup with cuvette (left), image of real device and a drop profile (right).

$2N_AC_0\Delta E\sqrt{(D_{eff})}/\sqrt{\pi}$.

By using linear fitting of the surface tension data versus time, the effective diffusivity of the particles (D_{eff}) is calculated and compared with the Stokes-Einstein equation for free diffusion ($D_0 = k_BT/6\pi\mu r$), which for 800 nm silica particles is 5.40259×10^{-13} m^2s^{-1}.

The effective diffusion D_{eff} due to the presence of an energy barrier U is related to the bare diffusion coefficient D_0 (without any adsorption barrier) by Eq. (6):

$$D_{eff} = D_0 \exp\left(-\frac{U}{k_BT}\right). \tag{6}$$

The bare diffusivity of the particle D_0 is calculated by using the Stokes-Einstein equation, where k_B is the Boltzmann constant (1.380649×10^{-23} J/K). This energy barrier is used to compare with the thermal energy. By using this equation, the energy barrier U is calculated from the effective diffusivity. Since the particles used are electrostatically stabilized, the energy barrier is likely to be of electrostatic origin and therefore we calculate the DLVO interactions near the interface [43].

With the modified short-time approximation model, provided that the bulk concentration is not significantly changed by the attachment of nanoparticles at the interface, we can fit the short-time data (less than 50 s) and obtain the effective diffusion coefficient and the energy barrier.

The original long-time adsorption model is described by Eq. (7) [46]:

$$t \to \infty : \gamma = \gamma_\infty + \frac{RTT_\infty^2}{C_0}\sqrt{\frac{\pi}{4Dt}}. \tag{7}$$

The symbols and units in Eq. (7) are consistent with the above equations, where the term γ_∞ is the intercept and $t^{-0.5}$ is the x coordinate.

There is a modified long-time approximation model [26], where Θ is the surface coverage (the fraction of the area of the interface occupied by nanoparticles) and Θ_{max} is the maximum coverage of the interface (assumed to equal 0.91 in this study, being the maximum hexagonal close-packing for a two-dimensional interface). With a material balance assumption for adsorbed nanoparticles at the interface, the dimensionless parameters can be rewritten to obtain the adsorption rate from the surface tension, as given in Eqs. (8) and (9),

$$\overline{k_a} \equiv k_a\frac{L}{D_0}, \tag{8}$$

$$L \equiv \frac{1}{N_AC_0S}. \tag{9}$$

Here, $S = \pi r^2$, and the relation between the modified adsorption rate $\overline{k_a}$ (obtained from surface tension experimental data) and the adsorption constant k_a (function of diffusion coefficient and specific interaction energy) is established. Using this approximation, we can derive Eq. (10),

$$\Theta = \Theta_{max} - \frac{K_1}{\sqrt{\tau}}, \tag{10}$$

where τ is the dimensionless time, and the intermediate parameter, K_1, is defined by Eq. (11),

$$K_1 = \Theta_{max}(\Theta_{max}/4.64\overline{k_a})^{0.5}. \tag{11}$$

The detachment energy is modified to take account of the maximum packing fraction, according to Ref. [26]:

$$|\Delta E| = \frac{\gamma_0 - \gamma_\infty}{\Theta_{max}}\pi r^2. \tag{12}$$

For the long-time approximation, the relation between surface tension (γ) and time (t) can be given as Eq. (13):

$$\gamma = \gamma_\infty + \frac{K_1|\Delta E|}{(\pi r^2)^2N_AC_0}\sqrt{\frac{1}{D_{eff}t}}. \tag{13}$$

We can see $\gamma \propto (1/\sqrt{t})$ and the proportional gradient 'Grad' is given by Eq. (14):

$$Grad = \frac{K_1|\Delta E|}{(\pi r^2)^2N_AC_0\sqrt{D_{eff}}}. \tag{14}$$

Thus, K_1 can be calculated with the linear fitting results of late-stage surface tension data, which is an intermediate parameter given knowledge of the adsorption energy, particle radius, and bulk concentration. The k_a can be obtained from the relationship between K_1 and $\overline{k_a}$ as Eqs. (10) and (11). Finally, with the conversion rule, the adsorption rate constant, k_a, can be obtained.

Therefore, the particle adsorption constant can be calculated to analyze the overall rate of particle adsorption. The maximum value of the interaction energy, ϕ, attributed to specific particle-interface interactions, ϕ_b, may be approximately inferred from k_a as Eq. (15):

$$k_a \cong \frac{D}{r}\sqrt{\frac{\phi_b}{\pi k_BT}}\exp\left(-\frac{\phi_b}{k_BT}\right). \tag{15}$$

In this study, to estimate k_a from the rate data, the long-time approximation surface tension data is fitted versus $t^{-0.5}$, from 50 s to the equilibrium state (with different samples) using unmodified commercial silica (SiO_2) nanoparticles, along with chemically esterified 'SiO-butane', and 'SiO-hexane' nanoparticles.

3. Results and discussion

3.1. Equilibrium layer compression and collapse

An illustrative example of a typical Π-A isotherm, obtained from the compression of the SiO-butane monolayer, is presented in Fig. 2. Examples of repeated compression and expansion cycles of SiO-butane along with the SiO-hexane particles are shown within the ESM (see Fig. S3). The SiO-butane particle system serves as an example case for elucidating pressure-area isotherms, as it unambiguously demonstrates the formation and collapse points of the layer, along with their intricate relationship to the emergence of a particle network, as shown in Fig. 2.

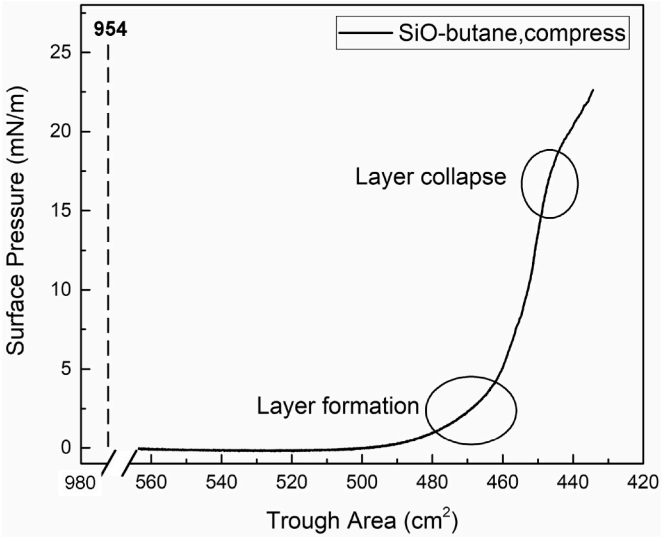

Fig. 2. Pressure-area (Π-A) isotherm of the SiO-butane silica particle monolayer with water. Highlighted in circles are the points of layer formation and collapse. The dotted line denotes the theoretical hexagonal close packing area, assuming a complete monolayer (954 cm^2).

Furthermore, the unmodified 800 nm SiO_2 particles failed to form a consistent monolayer on the subphase, despite utilizing a volume five times greater than that of SiO-butane. Consequently, these findings are omitted from the reported results. It is conceivable that the contact angle of the unmodified particles is comparatively small, resulting in most particles becoming submerged beneath the liquid interface during the monolayer formation process. This immersion precludes the particles from maintaining a stable configuration with a narrow contact line.

The SiO-butane particle layer exhibits a predictable trend in its behavior. As the trough area is gradually narrowed to a critical threshold, the particle rafts coalesce into a single, interconnected layer. This transition generates a lateral force [47], resulting in a sharp increase in surface pressure [48]. If the compression continues and the area is further diminished, a second critical point emerges. At this point, the layer collapses, and the particles are either expelled into the bulk medium or forced into a folded structure [49–51].

The relative abruptness of monolayer formation and collapse serves as a valuable indicator for understanding the homogeneity or aggregated nature of particle networks [49]. There is a 'monolayer region' between the highlighted points of layer formation and collapse. However, it is not truly a monolayer for those particles. Silica is nominally hydrophilic and the interparticle interactions will be dominated by symmetric bulk fluid electrostatics (such as DLVO [52]). The sudden, steep surge in surface pressure per unit area reduction suggests that the initial particle rafts rapidly reconfigure into a unified network with minimal lateral resistance, seeking to minimize the free energy state. Importantly, the area recorded at the collapse point is approximately half the theoretical close-packed area for a monolayer of the deposited mass of SiO-butane particles.

Thus, the theoretical hexagonal close-packed area position was analyzed for all systems, as given in Fig. 3, where the actual occupied area on layer collapse is recorded as a percentage of a pure HCP monolayer for SiO-butane and SiO-hexane layers. Different concentrations of MIBC were also added to the subphase to lower the surface tension, thereby facilitating the measurement of particle adsorption. To facilitate a comparative analysis, relative packing areas are utilized, which represent the ratio between the experimental packing area and the theoretical hexagonal close-packing area.

As in the case of pure SiO-butane, the experimental close-packing position for all systems deviates from the theoretical HCP position. This discrepancy is likely attributable to particle aggregation leading to overlap, or dispersion into the subphase. This observation suggests that some particles may not align perfectly within a monolayer and may instead be stacked or aggregated during the compression process. The SiO-hexane layers were much closer to the HCP monolayer than the SiO-butane, inferring greater layer stability for the more hydrophobic particles.

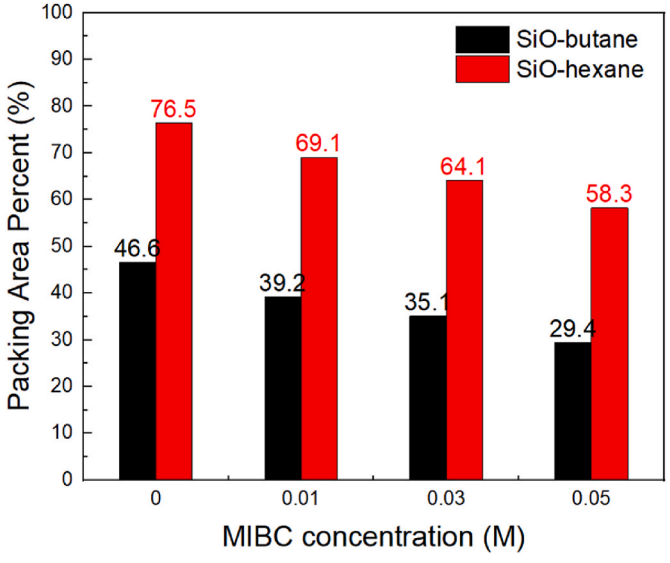

Fig. 3. Relative hexagonal close-packed (HPC) area percentage of SiO-butane and SiO-hexane formed on a Langmuir trough, and comparison with different concentrations of MIBC.

Furthermore, MIBC is observed to reduce the relative packing percentage in both systems as its concentration is increased, suggesting some interaction between MIBC and the particle layers. MIBC is a common frother agent added to aid bubble stability in froth flotation systems, and primarily is considered to interact at the air-water interface, rather than solid-liquid interface. As a short chain alcohol, it is not thought to adsorb to a significant extent onto the hydrophobic particles themselves. The fact that collapse areas reduce slightly with both particle systems may suggest either some level of adsorption and aggregation with the particles in the bulk or, perhaps more likely, its presence at the interface during compression disrupts longer order particle structures in the layer. Indeed, Bournival et al. [53] measured similar types of collapse reductions with MIBC and hydrophobized glass, determining that it acts as an interfacial dispersant. Also, as MIBC is soluble in these concentrations, its dynamic surface concentration will reduce as the barriers compress, and so its presence should not directly influence the collapse areas. Nonetheless, for the SiO-hexane layers at least, the small reduction in collapse areas for moderate concentrations of MIBC infers a relatively weak interaction.

To further explore systems directly correlated with the surface tension investigations, a comparison of SiO-butane and SiO-hexane monolayers with 0.05 M MIBC concentrations is shown in Figs. 4 and 5, where extracted layers using a wafer subphase were imaged with scanning electron microscopy (SEM). Other results of SiO-butane and SiO-hexane under low and high surface pressures with different magnifications are presented within the ESM (Figs. S4–S7).

For SiO-butane particles, it is evident that a degree of aggregation is present at low surface pressures, with this aggregation intensifying at higher pressures. This observation explains the significant deviation of experimental data from the theoretical HCP result. In contrast, SiO-hexane particles exhibit less extensive aggregation during compression, resulting in a packing that aligns closely with the theoretical HCP area.

The maximum surface pressure attained during compression decreases with increasing MIBC concentration, as shown in Fig. 6. This decrease is accompanied by a corresponding shift in the packing position. Notably, the compression curves of SiO-butane and SiO-hexane exhibit distinct characteristics. The SiO-hexane curve displays a more linear profile, lacking a pronounced inflection point indicative of layer formation and collapse, as observed in SiO-butane. Additionally, the surface pressure increases more rapidly and reaches higher values for SiO-hexane compared to SiO-butane, suggesting the presence of longer-range aggregates and a less distinct multilayer structure.

The occurrence of aggregation and overlap during the compression process is evident, and becomes more prominent with higher concentrations of MIBC. Even before and after compression, a slight aggregation of particles is observable, which becomes more significant with increasing MIBC concentrations (shown in Fig. 6). Among the three particle types, SiO-hexane particles exhibit the largest contact angle, rendering them the most hydrophobic. Both before and after compression, these particles consistently display favorable monolayer behavior, with most particles adopting a hexagonal arrangement. However, some larger aggregation clusters are still observed, with SiO-hexane particles exhibiting a moderate deviation in collapse area with increasing MIBC. As noted, it suggests some surface interactions between the MIBC and hydrophobic chain coating on the particles may reduce the stability of the particle layer [54].

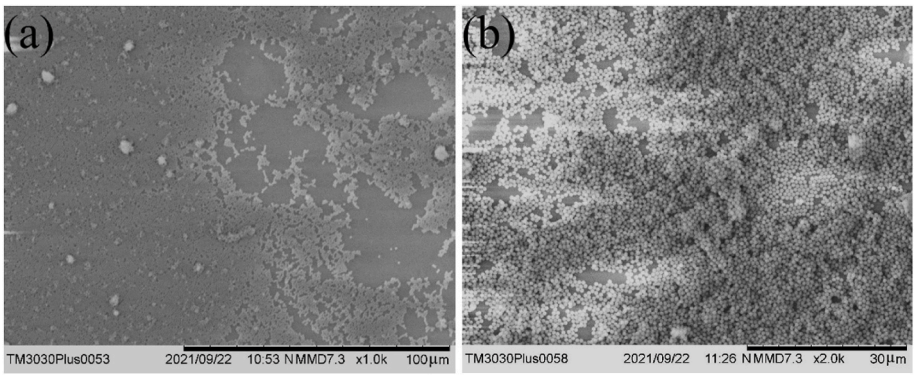

Fig. 4. Example SEMs of SiO-butane on 0.05M MIBC subphase under different surface pressure (a) low surface pressure of 0.3 mN/m and (b) high surface pressure of 15 mN/m.

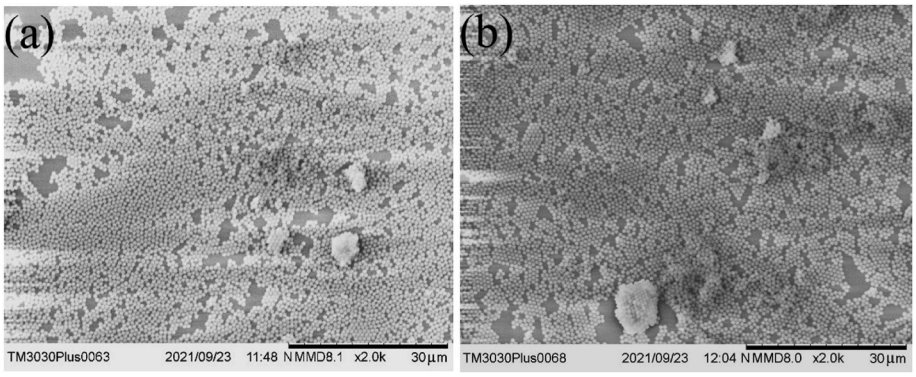

Fig. 5. Example SEMs of SiO-hexane on 0.05M MIBC subphase under different surface pressure (a) low surface pressure of 0.3 mN/m and (b) high surface pressure of 5 mN/m.

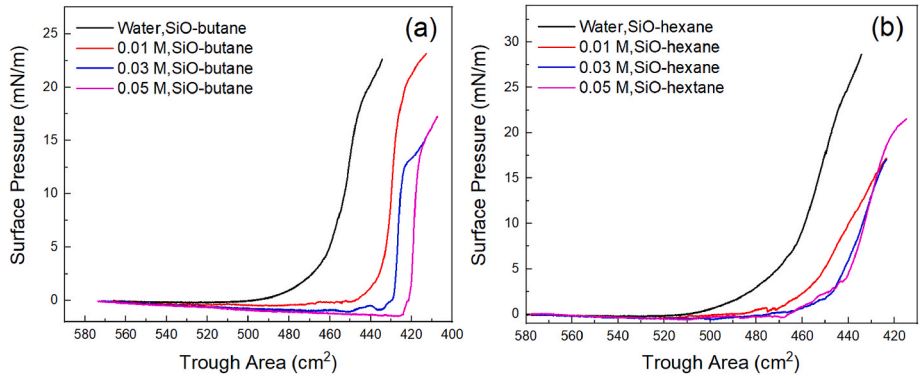

Fig. 6. Surface pressure versus trough area comparison of (a) SiO-butane and (b) SiO-hexane with different concentrations of MIBC.

3.2. Modeling adsorption dynamics via surface tension

To investigate the dynamic adsorption process at the air-water interface from the bulk fluid, pendant droplet experiments were conducted. Pendant drop surface tension versus time data of unmodified and esterified particles under 0.03M MIBC concentrations are shown in Fig. 7. The MIBC was added to facilitate more accurate measurements of nanoparticle adsorption from the apparent change in dynamic surface tension. Without MIBC, the surface did not deform with nanoparticle adsorption due to the high surface tension. At higher concentrations of MIBC, the droplets became unstable.

The initial surface tension of 0.03 M MIBC, measured without particles, is approximately 50 mN/m, depicted as a pink straight line in Fig. 7. Upon the introduction of particles, minor variations in the initial surface tension (at $t = 0$) were observed, albeit insignificant, potentially attributable to slight concentration fluctuations due to evaporation. However, the underlying trends are very clear. The dynamic surface tension of all three particle species decreases over time. Within the first 50 s, it undergoes a rapid decline, followed by a gradual reduction until a plateau equilibrium value is reached.

Furthermore, both the type and concentration of particles exert a significant influence on the final apparent surface tension. Specifically, at the lower concentration of 0.1 wt%, SiO-hexane particles exhibit the most prominent change compared to the other species. This observation suggests a more complete monolayer adsorption of the more hydrophobic particles, aligning with Langmuir trough studies on monolayer coverage. Additionally, at higher mass concentrations, the surface tension changes became more pronounced for all particle species. This

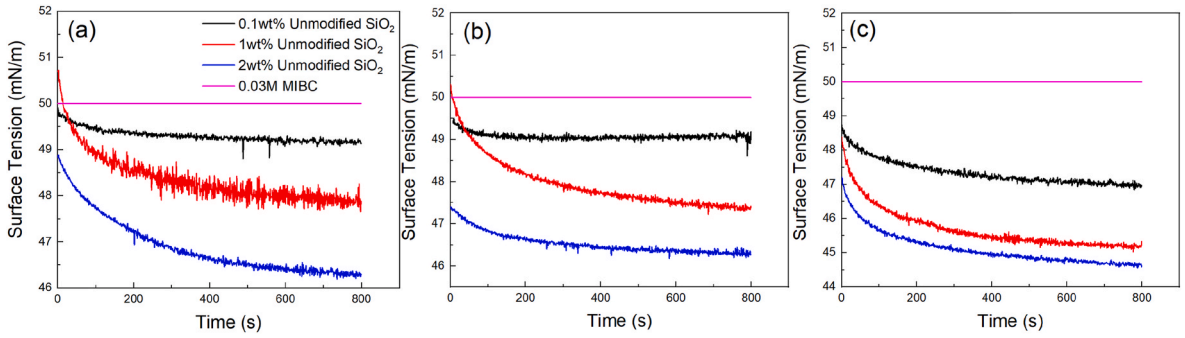

Fig. 7. The surface tension results of particles under different particle concentrations with 0.03 M MIBC. (a) Unmodified SiO_2, (b) SiO-butane, and (c) SiO-hexane. The black lines represent 0.1 wt% concentration, red lines represent 1 wt% and blue lines are 2 wt%. The pink line is the surface tension of pure 0.03 M MIBC.

difference may indicate greater overall particle coverage in all instances, leading to increased interfacial distortion, or potentially the emergence of multilayers.

However, given the stability of all particle species in the dispersion, there is limited incentive for multilayer adsorption from particles in the bulk. Instead, any observed changes are likely attributable to interfacial reorganization as the interfacial pressure increases, potentially manifesting as the formation of particle rafts, as evidenced by Langmuir trough data.

Since the particles used are electrostatically stabilized, the energy barrier is likely to be of electrostatic origin and therefore we calculate the DLVO interactions near the interface. Using the modified short-time approximation model and assuming that the bulk concentration was not significantly depleted by adsorption to the interface, we fitted the short-time data (<50 s) to obtain the effective diffusion coefficient and the energy barrier. Example results of the linear fitting of short-time and long-time approximation of SiO-hexane are shown in Fig. 8. The effective diffusion coefficients and energy barriers for all systems are summarized in Table 1, while detailed results of all short-time linear fits are provided in the ESM (Fig. S8).

The intercepts are the initial pure solution concentrations, and they are all close to 50 mN/m, which is the 0.03M MIBC initial surface tension. The energy barrier (U/k_BT) is calculated from the effective diffusion (D_{eff}), both of which are given in Table 1. To further illustrate these differences between particle systems, both D_{eff} and U/k_BT are plotted in Fig. 9 against concentration, showing that the adsorption energy barrier increases slightly with particle hydrophobicity and with particle concentration (with correlated reduction in D_{eff}).

For particles at higher concentrations and with higher hydrophobicity, their thermal energy is insufficient to overcome the energy barrier [30]. This underscores the inadequacy of diffusion alone in driving particle adsorption. Diffusion is significantly influenced by ΔE, the change in interfacial contact energy upon adsorption. This energy change, ΔE, is more pronounced for hydrophobic particles. Typically, this energy is associated with detachment, but it may also pose a barrier to initial adsorption.

Once particles establish a three-phase contact line with the droplet, their energy is elevated if the contact angle deviates significantly from the minimum energy state. This results in an escalated energy barrier, U. However, the magnitude of U is significantly smaller than ΔE (by several orders of magnitude) rendering the increase in the energy barrier relatively minor. Despite the larger adsorption energy barrier, the quantity of adsorbed particles can still be augmented [55], as evident in the equilibrium dynamic surface tension. As the adsorption of particles increases, the equilibrium dynamic surface tension exhibits lower values.

The investigation of the energy barrier relies on Eq. (4), presupposing that diffusion primarily governs particle behaviors. Analyzing this equation with identical data sets reveals intriguing insights. As wettability shifts towards greater hydrophobicity, ΔE rises for hydrophobic particles, theoretically leading to a decrease in D_{eff} if the curve maintains its gradient. For nanoparticles solely influenced by diffusion, one would expect a quadratic increase in gradient to yield a larger observed D_{eff} with altered wettability. However, our observations contradict this, indicating that particle behavior is not solely dictated by diffusion but rather by a more intricate mechanism. This complexity likely includes factors like the mixed diffusion-kinetic process [46], particularly evident during the initial stages of adsorption for larger colloidal particles, such as the 800 nm silica particles used in this study.

The diffusion coefficient of the 800 nm silica particles is minimal in comparison to values reported in studies involving particles below 100 nm [26,44]. For such nanoscopic sizes, diffusion is indeed the governing factor, but its influence wanes for larger particles, as exemplified by our 800 nm specimens. Notably, these larger particles are also subject to gravity and buoyancy, which contribute to surface deformation. Potential dynamic effects arising from droplet injection also play a role. For such colloids on the upper size limits, the inertia imparted by droplet

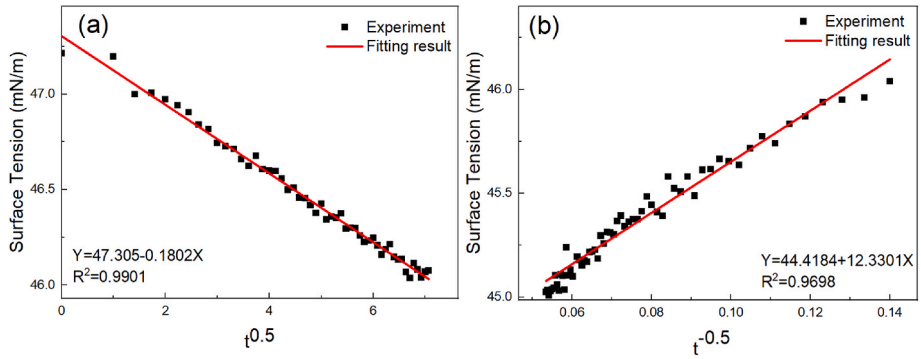

Fig. 8. (a) Modified short-time approximation linear fitting of surface tension versus $t^{0.5}$ and (b) modified long-time approximation linear fitting of surface tension versus $t^{-0.5}$ of SiO-hexane in 2 wt%.

Table 1
Modified short time approximation linear fitting results of surface tension versus $t^{0.5}$.

Cases	Intercept (mN/m)	Deviation (mN/m)	Gradient (mN/m.s$^{0.5}$)	Deviation (mN/m.s$^{0.5}$)	R^2	$D_{eff} \times 10^{-30}$ (m^2/s)	U/k_BT
0.1 wt% Unmod. SiO_2	49.853	0.0146	−0.039	0.0029	0.785	230.62	35.39
0.1 wt% SiO-butane	48.617	0.0183	−0.063	0.0036	0.857	5.11	39.20
0.1 wt% SiO-hexane	48.767	0.0234	−0.107	0.0047	0.913	0.89	40.95
1 wt% Unmod. SiO_2	50.876	0.0286	−0.226	0.0057	0.969	75.03	36.51
1 wt% SiO-butane	50.435	0.0181	−0.192	0.0036	0.982	0.48	41.57
1 wt% SiO-hexane	48.505	0.0257	−0.237	0.0051	0.977	0.043	43.97
2 wt% Unmod. SiO_2	49.037	0.0160	−0.123	0.0032	0.967	5.58	39.11
2 wt% SiO-butane	47.491	0.0144	−0.061	0.0029	0.901	0.012	45.25
2 wt% SiO-hexane	47.305	0.0128	−0.180	0.0026	0.990	0.0062	45.91

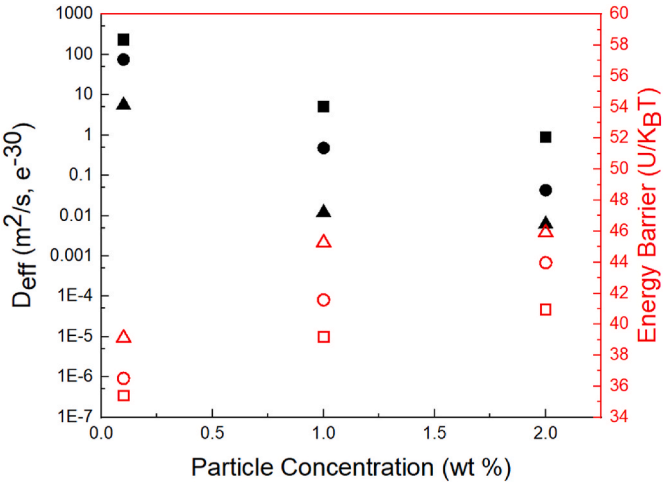

Fig. 9. Calculated effective diffusion coefficients (D_{eff}) and interfacial energy barriers (U/k_BT) from the modified short-time approximation model. Square symbols are unmodified SiO_2, circles SiO-butane, and triangles SiO-hexane. Black solids are the effective diffusion coefficients (left hand axis) and red hollow symbols are the energy barriers (right hand axis).

formation [56] may even aid adsorption, given the particles' unbalanced state. Our findings reveal a formidable energy barrier that cannot be surmounted by diffusion alone. Furthermore, the short-term effective diffusion coefficient underscores that a diffusion-only mechanism is inadequate to explain colloidal adsorption, especially for larger particles. This conclusion is reinforced by the fact that the model used to calculate D_{eff} is itself based solely on a diffusion mechanism, highlighting its limitation.

To investigate rate variations further, we analyzed long-term data using the alternative model (pertaining to data collected after 50 s, representative of the later stages). The comprehensive results from this long-term approximation of surface tension data are summarized in Table 2. The detailed results of all cases for the long-time linear fitting are shown in the ESM (Fig. S9).

The intercept represents the calculated equilibrium surface tension, γ^{eq}, which arises when particles occupy the liquid-gas interface at equilibrium. Notably, γ^{eq} diminishes with increasing particle concentrations and hydrophobicity. Intriguingly, the R^2 value also rises with particle concentrations and hydrophobicity, suggesting a closer alignment of the data with the long-term approximation model. Potentially, a concentration of 0.1 wt% may be insufficient to form a complete hydrophobic colloidal particle layer, leaving the drop interface incompletely occupied, thereby preventing the data from reaching an equilibrium state In general, the gradient of the fit increases with concentration, although a few anomalies are observed in the case of SiO-butane. The tabulated data unequivocally demonstrate that the adsorption rate constant, k_a, generally significantly increases with particle concentration and hydrophobicity. For a more intuitive understanding, k_a rate constants are plotted against concentration for all systems in Fig. 10.

As hydrophobicity increases, adsorption rates are enhanced by several orders of magnitude, far exceeding those of untreated silica particles. This phenomenon is attributable primarily to the increase in

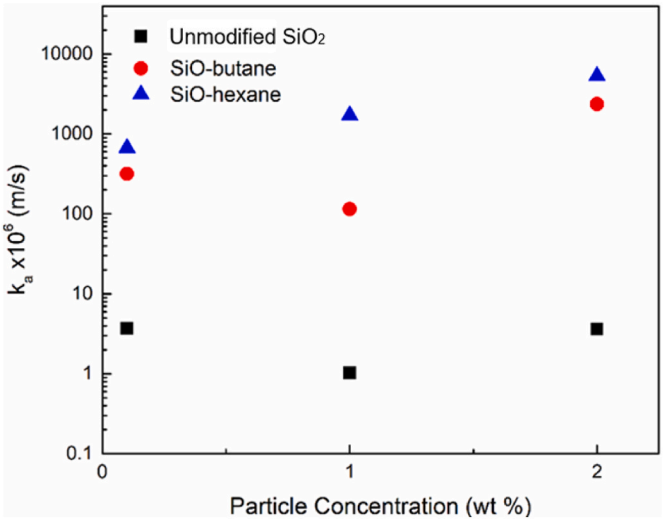

Fig. 10. Adsorption rates of nanoparticles using the long-time approximation model.

Table 2
Modified long-time approximation linear fitting results of surface tension versus $t^{-0.5}$.

Cases	Intercept (mN/m)	Deviation (mN/m)	Gradient (mN/m.s$^{0.5}$)	Deviation (mN/m.s$^{0.5}$)	R^2	$K_1 \times 10^{-5}$	$k_a \times 10^6$ (m/s)
0.1 wt% Unmod SiO_2	49.1127	0.02224	3.3168	0.21282	0.709	34.51	3.715
0.1 wt% SiO-butane	47.8404	0.05196	2.6265	0.44409	0.404	3.734	317.3
0.1 wt% SiO-hexane	47.0301	0.01947	7.3120	0.20309	0.896	2.568	671.0
1 wt% Unmod. SiO_2	47.5625	0.02548	13.3653	0.33129	0.823	207.6	1.027
1 wt% SiO-butane	46.9715	0.01125	16.4352	0.14623	0.973	19.63	114.8
1 wt% SiO-hexane	44.7052	0.01326	16.4118	0.17240	0.962	5.081	1714
2 wt% Unmod. SiO_2	45.6998	0.01499	19.9253	0.20995	0.952	156.2	3.627
2 wt% SiO-butane	46.1648	0.00742	6.5348	0.08790	0.956	6.112	2370
2 wt% SiO-hexane	44.4184	0.01014	12.3301	0.12609	0.969	4.074	5331

detachment energy with higher contact angles, facilitating statistically more adsorption versus desorption events at the interface. The impact of concentration on k_a is more complex. There are significant increases in adsorption rates between 0.1 and 2 wt% for SiO-butane and SiO-hexane, although the rate enhancement is lower than would be expected given 20-fold increase in particle number. Indeed, for both unmodified and SiO-butane particles, a minimum in adsorption is observed at 1 wt%, indicating a complex interaction with concentration. Notably, the adsorption rate for unmodified particles does not return to the level observed at 0.1 wt% even after reaching 2 wt%, suggesting greater competition for these weaker adsorbing species. The overall trend with concentration aligns with the findings of Bizmark et al. [26] where a 10 × concentration increase led to only a 3-fold enhancement in adsorption rates.

The long-time approximation model provides quantitative insights into the profound influence of hydrophobicity on particle adsorption, particularly in crowded surface environments. For 0.1 wt% droplets, SiO-hexane exhibits a k_a value 181 × higher than that of unmodified SiO_2, and this ratio soars to 1470 at 2 wt%. These remarkable differences highlight the dramatic impact of hydrophobicity on adsorption rates, which appears to markedly outweigh the influence of concentration. These observations may be attributed to the competition among particles for adsorption sites, as described by the mixed diffusion-kinetic theory [46], particularly when concentrations are significantly elevated. This competition is most likely offset by the concurrent increase in particle numbers from 1 to 2 wt%. Furthermore, the possibility of multilayers cannot be discounted, as previous work has shown with Langmuir trough results. Multilayers can distort the interface, thereby influencing the apparent surface tension, which can be analyzed through droplet morphology.

It is important to compare the apparent contrasting results on the influence of hydrophobicity from the shot-term and long-term adsorption modelling. Data from the short-term fitting indicated a reduced effective diffusivity for the most hydrophobic particles, inferring a retardation of their mobility to the interface. Such differences may suggest some slight aggregation of the hydrophobic particles in the droplet. Nevertheless, these effects are dominated by the influence of hydrophobicity on the robustness of the interface on long-time data, and statistical reduction in detachment efficiency. Highly hydrophobic SiO-hexane particles, for instance, form a robust and persistent monolayer that resists desorption and exhibits almost monolayer structure. This well-ordered interfacial layer leads to a high apparent efficiency in surface tension reduction, making the adsorption notably pronounced. In contrast, although unmodified SiO_2 and SiO-butane particles may exhibit higher effective diffusivity, this is offset by their inferior interfacial stability and tendency toward multilayer adsorption. This results in a larger fraction of particles either being detached within the bulk phase or with multilayers reducing the total extent of the particle network, thereby reducing the observable adsorption rates. Over extended timescales, early-stage diffusivity becomes less consequential, and adsorption outcomes are dominated instead by interfacial stability—a property dictated primarily by hydrophobicity.

Additionally for the relatively large colloids (800 nm) investigated in this study, gravitational effects serve as a secondary driving force during the early adsorption stage, efficiently transporting particles to the liquid-gas interface and diminishing the relative importance of diffusive transport [57]. Consequently, the key factor determining the overall adsorption rate shifts to the intermediate and final stages, which are governed by the structure and stability of the adsorbed particle layer. To evidence this, we consider the Péclet number, defined here as $Pe = (\rho_P - \rho_f) g \pi d^4 / (6 k_B T)$, which describes the relative importance of gravitational settling to diffusion (subscripts 'p' and 'f' donate particle and fluid, while 'd' is the particle diameter). The $Pe \approx 0.62$ in this study, where a Pe number of ~1 indicates that the gravitational settling rate is comparable to the diffusive transport rate. Therefore, sedimentation contributes importantly to particle delivery to the vicinity of the interface.

Thus, a proposed mixed adsorption mechanism for large silica particles can be summarized. In the early stage, adsorption is governed by a combination of diffusion, gravitational settling, and electrostatic interactions. The electrostatic effects influence both particle-interface interactions and the formation of closely packed interfacial structures. The relative contributions of diffusion and settling can be quantified using the Péclet number, wherein the hindering effect of hydrophobicity on diffusion becomes less dominant as the Péclet number increases. Over longer timescales, adsorption is dominated by hydrophobicity, which directly determines the structure of the adsorbed layer. Both the efficiency of particle adsorption and the apparent reduction in surface tension are enhanced with increasing particle hydrophobicity.

4. Conclusions

This study investigated the adsorption dynamics of 800 nm colloidal particles at fluid interfaces through drop adsorption experiments and Langmuir-Blodgett trough measurements, complemented by short and long-term modeling to calculate energy barriers and adsorption rates. The research aimed to elucidate how particle hydrophobicity and concentration govern the formation of particle monolayers and the nature of these layers.

From LB trough results, hydrophilic particles were observed to be more prone to detach from the interface and return to the bulk fluid, which may hinder the adsorption of other particles. Although these particles may still be adsorbed when immersed in the bulk phase, the interface deformation may be too subtle for experimental equipment to detect significant surface distortions. Studies of butanol ('SiO-butane') and hexanol ('SiO-hexane') esterified particles showed clear surface compression and contrasting behavior. The SiO-butane particles formed weaker particle layers that underwent partial collapse into multilayers with compression, leading to formations much below hexagonal close-packed (HPC) monolayer estimates. Alternatively, the SiO-hexane particles exhibited much improved monolayer behavior and longer-range stability. Further measurements with methyl isobutyl carbinol (MIBC) used as co-surfactant in surface tension measurements suggested some weak interaction between the MIBC and particles. Estimated HCP areas slightly reduced as MIBC increased, perhaps indicative of some particle aggregation at the interface or that the MIBC acted as an interfacial dispersant.

Droplet surface tension measurements were used to reveal adsorption dynamics, where hydrophobic particles induced significant changes in surface tension during adsorption, consistent with Langmuir trough observations of monolayer coverage. Short-term approximation modeling and energy barrier calculations provided insights into diffusion and other mechanisms affecting adsorption dynamics. Hydrophobic particles exhibited higher desorption energy and larger contact areas, facilitating stable monolayer formation, while hydrophilic particles showed greater detachment propensity, limiting adsorption stability. Despite greater calculated energy barrier and reduced diffusion, long-term rate modeling indicated the adsorption rates of the most hydrophobic SiO-hexane particles were significantly greater than either the SiO-butane particles or unmodified particles. Indeed, adsorption coefficients (k_a) for SiO-hexane particles were ~200 × greater than for unmodified particles at low 0.1 wt% particle concentrations and over 1000 × greater at 2 wt%. The role of particle concentration was more complex, with effects dominated by hydrophobicity. Although the adsorption rate generally increased with concentration, the data suggest a critical transition point at intermediate hydrophobicity, where particle detachment is significantly reduced. Importantly also, results demonstrated that a diffusion-only mechanism is inadequate to explain the adsorption dynamics of these larger colloids. The early-stage behavior is attributed to both diffusion and a gravity-driven effect, the relative importance of which can be quantified by the Péclet number. Overall,

this study provided quantitative insights into the profound influence of hydrophobicity on particle adsorption, particularly in crowded surface environments. Extending these insights to biomedical and materials science applications, such as nanomaterials and drug carriers, holds significant promise for advancing related technologies.

CRediT authorship contribution statement

Hangyu Chen: Writing – original draft, Methodology, Investigation, Formal analysis, Data curation, Conceptualization. **Xiaodong Jia:** Writing – review & editing, Supervision, Software, Resources. **Michael Fairweather:** Writing – review & editing, Supervision, Software, Resources. **Timothy N. Hunter:** Writing – review & editing, Supervision, Resources, Project administration, Methodology, Conceptualization.

Declaration of competing interest

The authors declare that they have no known competing financial interests or personal relationships that could have appeared to influence the work reported in this paper.

Acknowledgements

Thanks are given to Ben Douglas for experimental support. The authors would like to also acknowledge Stuart Micklethwaite and the Leeds Electron Microscopy and Spectroscopy (LEMAS) Centre for help in conducting the SEM analysis.

Appendix A. Supplementary data

Supplementary data to this article can be found online at https://doi.org/10.1016/j.jciso.2025.100154.

Data availability

Data will be made available on the University of Leeds White Rose repository, at https://doi.org/10.5518/1746.

References

[1] M.M. Eissa, M.M. Rahman, N. Zine, N. Jaffrezic, A. Errachid, H. Fessi, A. Elaissari, Reactive magnetic poly (divinylbenzene-co-glycidyl methacrylate) colloidal particles for specific antigen detection using microcontact printing technique, Acta Biomater. 9 (3) (2013) 5573–5582.
[2] O. Cayre, V.N. Paunov, O.D. Velev, Fabrication of asymmetrically coated colloid particles by microcontact printing techniques, J. Mater. Chem. 13 (10) (2003) 2445–2450.
[3] M. Xiao, A. Xu, T. Zhang, L. Hong, Tailoring the wettability of colloidal particles for Pickering emulsions via surface modification and roughness, Front. Chem. 6 (2018) 225.
[4] D. Venkataramani, A. Tsulaia, S. Amin, Fundamentals and applications of particle stabilized emulsions in cosmetic formulations, Adv. Colloid Interface Sci. 283 (2020) 102234.
[5] A. Jamburidze, A. Huerre, D. Baresch, V. Poulichet, M. De Corato, V. Garbin, Nanoparticle-coated microbubbles for combined ultrasound imaging and drug delivery, Langmuir 35 (31) (2019) 10087–10096.
[6] J.D. Berry, M.J. Neeson, R.R. Dagastine, D.Y. Chan, R.F. Tabor, Measurement of surface and interfacial tension using pendant drop tensiometry, J. Colloid Interface Sci. 454 (2015) 226–237.
[7] D. Jones, The free energies of solid-liquid interfaces, J. Mater. Sci. 9 (1) (1974) 1–17.
[8] D. Dedovets, Q. Li, L. Leclercq, V. Nardello-Rataj, J. Leng, S. Zhao, M. Pera-Titus, Multiphase microreactors based on liquid–liquid and gas–liquid dispersions stabilized by colloidal catalytic particles, Angew. Chem. Int. Ed. 61 (4) (2022) e202107537.
[9] M.S. Manga, T.N. Hunter, O.J. Cayre, D.W. York, M.D. Reichert, S.L. Anna, L. M. Walker, R.A. Williams, S.R. Biggs, Measurements of submicron particle adsorption and particle film elasticity at oil–water interfaces, Langmuir 32 (17) (2016) 4125–4133.
[10] X. Ji, X. Wang, Y. Zhang, D. Zang, Interfacial viscoelasticity and jamming of colloidal particles at fluid-fluid interfaces: a review, Rep. Prog. Phys. 83 (12) (2020) 126601, 126601.
[11] J. Bergfreund, P. Bertsch, P. Fischer, Effect of the hydrophobic phase on interfacial phenomena of surfactants, proteins, and particles at fluid interfaces, Curr. Opin. Colloid Interface Sci. 56 (2021) 101509.
[12] S. Stock, R. von Klitzing, Microgels at droplet interfaces of water-in-oil emulsions—Challenges and progress, Curr. Opin. Colloid Interface Sci. 58 (2022) 101561.
[13] B.P. Binks, Particles as surfactants-similarities and differences, Curr. Opin. Colloid Interface Sci. 7 (1–2) (2002) 21–41.
[14] B.P. Binks, S.O. Lumsdon, Influence of particle wettability on the type and stability of surfactant-free emulsions, Langmuir 16 (23) (2000) 8622–8631.
[15] H. Zhao, Y. Yang, Y. Chen, J. Li, L. Wang, C. Li, A review of multiple Pickering emulsions: solid stabilization, preparation, particle effect, and application, Chem. Eng. Sci. 248 (2022) 117085.
[16] L. Xu, G. Han, J. Hu, Y. He, J. Pan, Y. Li, J. Xiang, Hydrophobic coating-and surface active solvent-mediated self-assembly of charged gold and silver nanoparticles at water–air and water–oil interfaces, Phys. Chem. Chem. Phys. 11 (30) (2009) 6490–6497.
[17] O.N. Oliveira Jr., L. Caseli, K. Ariga, The past and the future of Langmuir and Langmuir–Blodgett films, Chem. Rev. 122 (6) (2022) 6459–6513.
[18] R. Lathia, C.D. Modak, P. Sen, Two modes of contact-time reduction in the impact of particle-coated droplets on superhydrophobic surfaces, Droplet 2 (4) (2023) e89.
[19] O.S. Deshmukh, D. Van Den Ende, M.C. Stuart, F. Mugele, M.H. Duits, Hard and soft colloids at fluid interfaces: adsorption, interactions, assembly & rheology, Adv. Colloid Interface Sci. 222 (2015) 215–227.
[20] E. Guzmán, F. Martinez-Pedrero, C. Calero, A. Maestro, F. Ortega, R.G. Rubio, A broad perspective to particle-laden fluid interfaces systems: from chemically homogeneous particles to active colloids, Adv. Colloid Interface Sci. 302 (2022) 102620.
[21] C.O. Metin, J.R. Baran, Q.P. Nguyen, Adsorption of surface functionalized silica nanoparticles onto mineral surfaces and decane/water interface, J. Nanoparticle Res. 14 (11) (2012) 1–16.
[22] M. Bodik, M. Jergel, E. Majkova, P. Siffalovic, Langmuir films of low-dimensional nanomaterials, Adv. Colloid Interface Sci. 283 (2020) 102239.
[23] D.K. Schwartz, Langmuir-Blodgett film structure, Surf. Sci. Rep. 27 (7–8) (1997) 245–334.
[24] M. Safouane, D. Langevin, B. Binks, Effect of particle hydrophobicity on the properties of silica particle layers at the air− water interface, Langmuir 23 (23) (2007) 11546–11553.
[25] C. Kumar, S. Bhattacharjee, S. Srivastava, Shape anisotropy induced jamming of nanoparticles at liquid interfaces: a tensiometric study, Nanoscale Adv. 6 (18) (2024) 4683–4692.
[26] N. Bizmark, M.A. Ioannidis, D.E. Henneke, Irreversible adsorption-driven assembly of nanoparticles at fluid interfaces revealed by a dynamic surface tension probe, Langmuir. AcsJ.of Surf.;Coll. 30 (3) (2014) 710.
[27] Y. Fu, J. Frechette, Distinct contributions of particle adsorption and interfacial compression to the surface pressure of a fluid interface, Langmuir 40 (46) (2024) 24471–24483.
[28] M. Mahmoudvand, H. Vatanparast, A. Javadi, A. Kantzas, S. Burns, M. Dolgos, R. Miller, A. Bahramian, Evaluation of interfacial structure of self-assembled nanoparticle layers: use of standard deviation between calculated and experimental drop profiles as a novel method, Langmuir 40 (4) (2024) 2130–2145.
[29] F. Bashforth, J.C. Adams, An Attempt to Test the Theories of Capillary Action by Comparing the Theoretical and Measured Forms of Drops of Fluid, University Press, 1883.
[30] V.R. Dugyala, J.S. Muthukuru, E. Mani, M.G. Basavaraj, Role of electrostatic interactions in the adsorption kinetics of nanoparticles at fluid–fluid interfaces, Phys. Chem. Chem. Phys. 18 (7) (2016) 5499–5508.
[31] S. Parajuli, E.E. Ureña-Benavides, Fundamental aspects of nanocellulose stabilized Pickering emulsions and foams, Adv. Colloid Interface Sci. 299 (2022) 102530.
[32] Y. Gerelli, F. Camerin, S. Bochenek, M.M. Schmidt, A. Maestro, W. Richtering, E. Zaccarelli, A. Scotti, Softness matters: effects of compression on the behavior of adsorbed microgels at interfaces, Soft Matter 20 (17) (2024) 3653–3665.
[33] G.C. Yang, L. Jing, C.Y. Kwok, Y.D. Sobral, A comprehensive parametric study of LBM-DEM for immersed granular flows, Comput. Geotech. 114 (2019) 103100.
[34] D.M. Kaz, R. McGorty, M. Mani, M.P. Brenner, V.N. Manoharan, Physical ageing of the contact line on colloidal particles at liquid interfaces, Nat. Mater. 11 (2) (2012) 138–142.
[35] N. Ballard, A.D. Law, S.A.F. Bon, Colloidal particles at fluid interfaces: behaviour of isolated particles, Soft Matter 15 (6) (2019) 1186–1199.
[36] H. Chen, X. Jia, M. Fairweather, T.N. Hunter, Characterising the sedimentation of bidisperse colloidal silica using analytical centrifugation, Adv. Powder Technol. 34 (2) (2023) 103950.
[37] H. Chen, T.C. Sykes, O. Kivan, X. Jia, M. Fairweather, T.N. Hunter, Simulation of bidisperse colloidal centrifugal sedimentation using a mixture viscosity model, Phys. Fluids 35 (12) (2023) 123306.
[38] T.N. Hunter, E.J. Wanless, G.J. Jameson, Effect of esterically bonded agents on the monolayer structure and foamability of nano-silica, Colloids Surf. A Physicochem. Eng. Asp. 334 (1–3) (2009) 181–190.
[39] G.C. Ossenkamp, T. Kemmitt, J.H. Johnston, Toward functionalized surfaces through surface esterification of silica, Langmuir 18 (15) (2002) 5749–5754.
[40] M. Trau, B.S. Murray, K. Grant, F. Grieser, An ellipsometric study of thin films on silica plates formed by alkylchlorosilylation reagents, J. Colloid Interface Sci. 148 (1) (1992) 182–189.
[41] S.M.I. Saad, Z. Policova, A.W. Neumann, Design and accuracy of pendant drop methods for surface tension measurement, Colloids Surf. A Physicochem. Eng. Asp. 384 (1–3) (2011) 442–452.

[42] M. Peng, T.T. Duignan, C.V. Nguyen, A.V. Nguyen, From surface tension to molecular distribution: modeling surfactant adsorption at the air–water interface, Langmuir 37 (7) (2021) 2237–2255.
[43] V.B. Fainerman, A.V. Makievski, R. Miller, The analysis of dynamic surface tension of sodium alkyl sulphate solutions, based on asymptotic equations of adsorption kinetic theory, Coll.Surf.Physicochem.Eng.asp. 87 (1) (1994) 61–75.
[44] V.R. Dugyala, J.S. Muthukuru, E. Mani, M.G. Basavaraj, Role of electrostatic interactions in the adsorption kinetics of nanoparticles at fluid-fluid interfaces, Phys. Chem. Chem. Phys. : Phys. Chem. Chem. Phys. 18 (7) (2016) 5499–5508.
[45] S. Levine, B.D. Bowen, S.J. Partridge, Stabilization of emulsions by fine particles I. Partitioning of particles between continuous phase and oil/water interface, Colloids Surf. 38 (2) (1989) 325–343.
[46] J. Eastoe, J. Dalton, Dynamic surface tension and adsorption mechanisms of surfactants at the air–water interface, Adv. Colloid Interface Sci. 85 (2–3) (2000) 103–144.
[47] L.A. Pugnaloni, R. Ettelaie, E. Dickinson, Brownian dynamics simulation of adsorbed layers of interacting particles subjected to large extensional deformation, J. Colloid Interface Sci. 287 (2) (2005) 401–414.
[48] C. Monteux, J. Kirkwood, H. Xu, E. Jung, G.G. Fuller, Determining the mechanical response of particle-laden fluid interfaces using surface pressure isotherms and bulk pressure measurements of droplets, Phys. Chem. Chem. Phys. 9 (48) (2007) 6344–6350.
[49] S. Bordács, A. Agod, Z. Hórvölgyi, Compression of Langmuir films composed of fine particles: collapse mechanism and wettability, Langmuir 22 (16) (2006) 6944–6950.
[50] T.S. Horozov, B.P. Binks, R. Aveyard, J.H. Clint, Effect of particle hydrophobicity on the formation and collapse of fumed silica particle monolayers at the oil–water interface, Colloids Surf. A Physicochem. Eng. Asp. 282 (2006) 377–386.
[51] Z. Hórvölgyi, S. Németh, J.H. Fendler, Monoparticulate layers of silanized glass spheres at the water– air interface: particle– particle and particle– subphase interactions, Langmuir 12 (4) (1996) 997–1004.
[52] P. Hiemenz, R. Rajagopalan, Electrostatic and polymer-induced colloid stability. Principles of Colloid and Surface Chemistry, third ed., Marcel Dekker, New York, 1997, pp. 604–610.
[53] G. Bournival, X. Yang, S. Ata, The interaction of a bubble with a particle-laden interface in frother solutions, Colloids Surf. A Physicochem. Eng. Asp. 621 (2021) 126609.
[54] M. Xu, A. Vanderbruggen, N. Kupka, H. Zhang, M. Rudolph, Influence of MIBC on the surface-air nucleation and bubble-particle loading in graphite froth flotation, Miner. Eng. 185 (2022) 107714.
[55] S. Ferdous, M.A. Ioannidis, D.E. Henneke, Effects of temperature, pH, and ionic strength on the adsorption of nanoparticles at liquid–liquid interfaces, J. Nanoparticle Res. 14 (5) (2012) 1–12.
[56] T. Matsunaga, A. Södersten, S. Koshizuka, T. Hosaka, E. Ishii, Axisymmetric free-surface flow simulation using the moving surface mesh particle method and application to drop formation, J. Comput. Phys. 463 (2022) 111298.
[57] H.S. Wi, S. Cingarapu, K.J. Klabunde, B.M. Law, Nanoparticle adsorption at liquid-vapor surfaces: influence of nanoparticle thermodynamics, wettability, and line tension, Langmuir 27 (16) (2011) 9979–9984.